QUANTITATIVE IMAGING OF MIM DEBINDING AND SINTERING

David W. Yoel, Charles W. Miller, Jr.
and Robert K. Olson
Centorr/Vacuum Industries, Inc.
Stephen C. Bates
Thoughtventions Unlimited

ABSTRACT

Refined in-situ measurements of Metal Injection Molded parts during debinding and sintering using microscopic and macroscopic imaging are reported. Advances in digital imaging, illumination and filtering, optical access, and far focus microscopy have led to the capabilities that enable this type of optical process monitoring. Although some in-process diagnostics are currently available, most PIM process modifications are made by iteration based on properties of the finished part. Experiments microscopically monitoring debinding and sintering are reported, as are experiments macroscopically gauging part size during sintering. The onset of shrinkage for the specific experiments reported begin far below the sintering temperature and occur at a higher rate during the ramp to temperature than during the sinter soak.

INTRODUCTION

Metal Injection Molding (MIM) is used to efficiently make complex net shape parts from high temperature materials. The large amounts of binder used and the major changes in physical dimensions that result from sintering can cause parts to change shape unpredictably and to densify uncontrollably. Time consuming and costly iteration is most often used to improve MIM processing. In-situ diagnostics are needed to monitor MIM processing, to enable more rapid process development, and to enable Intelligent Process Control (IPC) techniques based on these diagnostics. This program combines microscopic and macroscopic optical imaging for in-situ monitoring of MIM processing. Advances in digital imaging, illumination and filtering, optical access, and far focus microscopy have led to the capabilities that enable this type of optical process monitoring.

PROGRAM OBJECTIVES

The rationale for the selection of quantitative imaging as part of an IPC program for PIM have

been discussed previously (1). The overall objectives of the current program are to:

1) Quantitatively image the debinding and sintering of MIM parts,
2) Correlate observations to theory,
3) Develop laboratory tools to accelerate debinding and optimize sintering, and
4) Develop Intelligent Process Control (IPC) technology for production systems.

The program is currently focused on the first objective.

EXPERIMENTAL APPROACH

The specific MIM material studied is 17-4PH stainless steel with a traditional thermoplastic binder (approximately 40% by volume). The parts are debound in a thermal vacuum environment and sintered in a partial pressure argon atmosphere in a graphite furnace following Centorr/Vacuum Industries' Injectavac™ process (2, 3, 4). In the current experiments, the debinding and sintering are conducted in separate systems to simplify the experimental setup. Later, a combined debind/sinter system shall be developed to properly duplicate the Injectavac™ process. During debinding, the parts are monitored microscopically. During the sinter cycle both microscopic and macroscopic images are acquired.

DEBINDING/MICROSCOPY EXPERIMENTS

Figure 1 describes the experimental setup for the debinding experiments. An MIM part is mounted on a sapphire setter plate and placed on a graphite pedestal in a glass vacuum flask and connected to a small mechanical vacuum pump. An electric heater is mounted below the flask and surrounded by insulation. A high intensity light source provides front surface illumination of the sample. A far field microscope attached to a video camera is mounted in front of the flask and connected to a personal computer with image processing hardware and software.

Figure 2 presents the profile for a typical experiment, with markings indicating the times and temperatures various images were acquired. A resolution of approximately 5 microns was achieved for these micro images, since the scale length of a pixel is about 3 microns, measured in separate and not exactly related tests. Figure 3a shows the baseline case of the initial condition of the part. Imaging system (not part) defects include horizontal scan line distortion across the lower portion of the image, and black dots that were found to be caused by dirt on the CCD window.

Figure 3b shows the same surface area at a temperature of 220°C, after the paraffin has been removed. The surface has changed from smooth to rough, indicated by a great deal of surface structure that has appeared in the later image. The small bright spots are thought to be a result of reflection from individual MIM particles that protrude from the surface. Continuous inspection of the video of the entire time interval shows that the surface area under inspection has not changed and the lighting has not changed. The unprocessed images require experience to interpret. Refinements in the image processing techniques utilized are required to make the appearance of surface image evolution more obvious.

Other microscopic images of the part at temperatures that lead to polymer removal show an

increase in visible microstructure - the fineness of the surface increases (Figure 3c). This would be expected by the final removal of all of the filling binder, leaving only metal particles in view.

SINTERING/GAUGING EXPERIMENTS

Figure 4 describes the experimental setup for the sintering experiments. The imaging system is identical to that used in the debinding tests. In the case of the gauging tests, a macroscopic lens is used whereas in the microscopy experiments, a far field microscope is attached. The furnace used is a Centorr/Vacuum Industries' Testorr™ furnace described previously (1). A key objective of the configuration selected is to minimize working distance while providing noninvasive optical access.

Prior to installation into the furnace, the brown parts' width is measured. Once installed in the furnace, an image is acquired - prior to the start of the sinter cycle - and stored in computer memory (Figure 5). The image is stored as a two-dimensional array of picture elements (pixels) of varying intensity. The array size (and thus spatial resolution) is determined by the video resolution (about 400 x 400 for standard video). The intensity resolution is determined by noise in the imaging system and the bit resolution of the image acquisition board.

Once stored in memory as a pixel array, the image can be enhanced using standard image processing techniques such as image averaging for noise reduction and edge detection for length measurement. The distance between any two points can be determined automatically as a function of the array coordinates of each point. Together, these capabilities permit accurate (to within a few percent) measurement of the dimensions of parts during MIM sintering, leading to quantitative shrinkage measurements of the parts being processed.

From a line profile of the initial room temperature image the part size can be estimated at .330"/180 pixels = 1.8×10^{-3} inches/pixel (Figure 6). Table 1 identifies typical measurements made at various times and temperatures. In Figure 7, these measurements are related to the temperature profile of the sintering experiment. This figure gives a clear description of the shrinkage of the part over the cycle of time and temperature. The part began to shrink at approximately 950°C during a 5°C/minute ramp and continued to shrink at a relatively constant rate of approximately 4.3×10^{-4} inches/minute or .13% of width/minute until the 1200°C sinter soak temperature was achieved. At sintering temperature, the rate of shrinkage fell to approximately 5×10^{-5} inches/minute or .015%/minute. At the end of the sinter period, power was shut off and the rate of shrinkage once again increased to 2.1×10^{-4} inches/minute or .065%/minute.

SINTERING/MICROSCOPY EXPERIMENTS

The furnace setup shown in Figure 4 that was used primarily for part gauging tests was also used to demonstrate microscopic imaging of parts during the sintering cycle. The microscopic imaging was done on a broken part as shown in Figure 8. The dark depressions result from non-uniform fracture of the part. The bright spots are again thought to be reflections of individual MIM particles. The surface was observed during a presinter ramp, and the surface could be seen to evolve. Higher intensity illumination is required to monitor the surface microscopically at sintering temperature. Detailed analysis has not been performed to date.

TABLE 1. SINTERING/GAUGING TESTS

Image No.	Elapsed Time (minutes)	Temp. (°C)	Width (Pixels)	Width (Inches)
0	0	38°	180	.330
10	350	734°	181	.332
11	380	880°	182	.334
12	412	1000°	176	.323
13	440	1136°	168	.308
14	482	1200°	166	.304
19	563	1200°	164	.300
20	573	1000°	163	.299
24	592	233°	161	.295

SUMMARY AND CONCLUSIONS

Thermal vacuum debinding of MIM parts can be visually observed on a microscopic scale. During paraffin removal, the surface appearance changes from smooth to rough and evolves over time, sometimes rapidly. During polymer removal, an increase in the microstructure of the surface is observed. Macroscopic gauging of part dimensions can be used for detailed studies of MIM sintering. Significant shrinkage occurred during the presinter ramp, and continued at a reduced rate during sintering. The shrinkage rate during post-sinter cooling was greater than during the sinter soak. Microscopic changes were observed during presintering. Further equipment refinements are required to monitor the sintering process microscopically.

Refined quantitative imaging of MIM debinding and sintering has been demonstrated. The next stage of the program will use this new tool for detailed studies of the thermal vacuum debinding and partial pressure sintering of MIM parts.

ACKNOWLEDGEMENTS

The authors wish to thank Advanced Forming Technology, Inc., Longmont, CO, for supplying the parts used in this study.

REFERENCES

1) D. Yoel, C. W. Miller, Jr. and R. K. Olson, "Image Acquisition And Analysis During Sintering: A Method Of Monitoring And Controlling P/M Part Characteristics", Vol. 4, Metal Powder Ind. Federation, Princeton, NJ, 1994, pp.85-94

2) D. Yoel, "C/VI Seeking to Expand MIM Materials Base", Metal Powder Report, June, 1994.

3) D. P. Duncavage and C.W.P. Finn, "Debinding and Sintering of Metal Injection Molded 316L Stainless Steel, Vol.5 Metal Powder Ind. Federation, Princeton, NJ 1993, pp.91-103

4) D. Duncavage , C.W.P. Finn and S. Donahue, "Debinding and Sintering of Low Carbon Stainless Steel MIM Parts", Metal Powder Report, May, 1992.

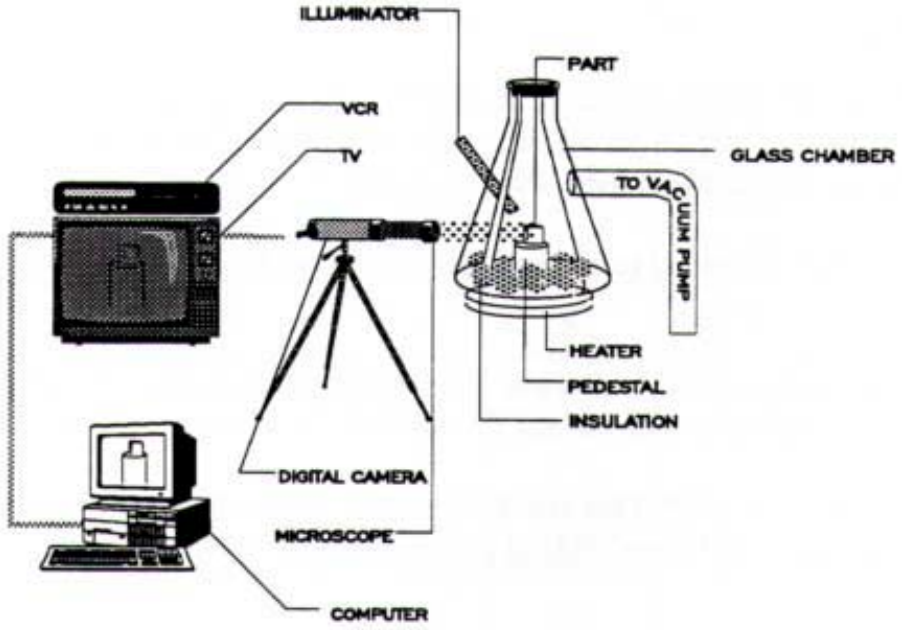

Figure 1. Debinding test setup.

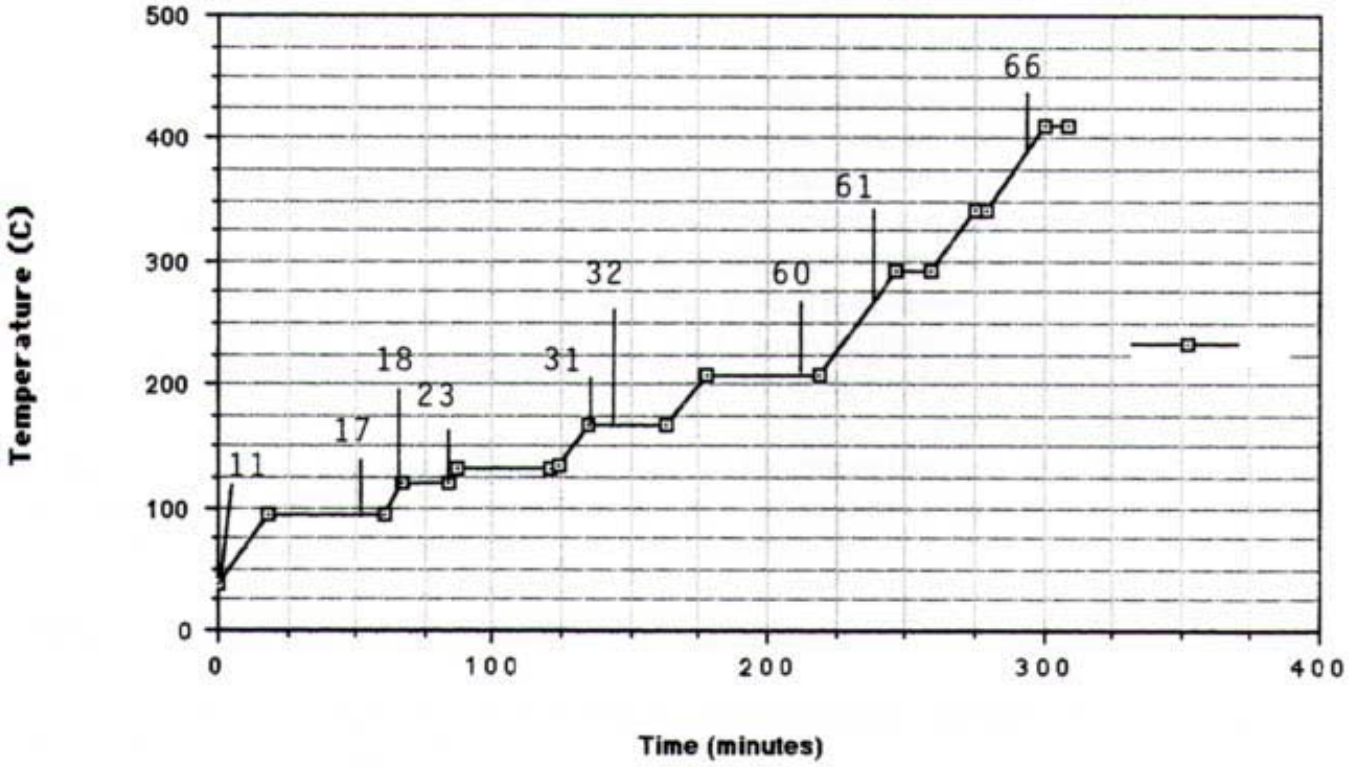

Figure 2. Debind cycle with image numbers indicated.

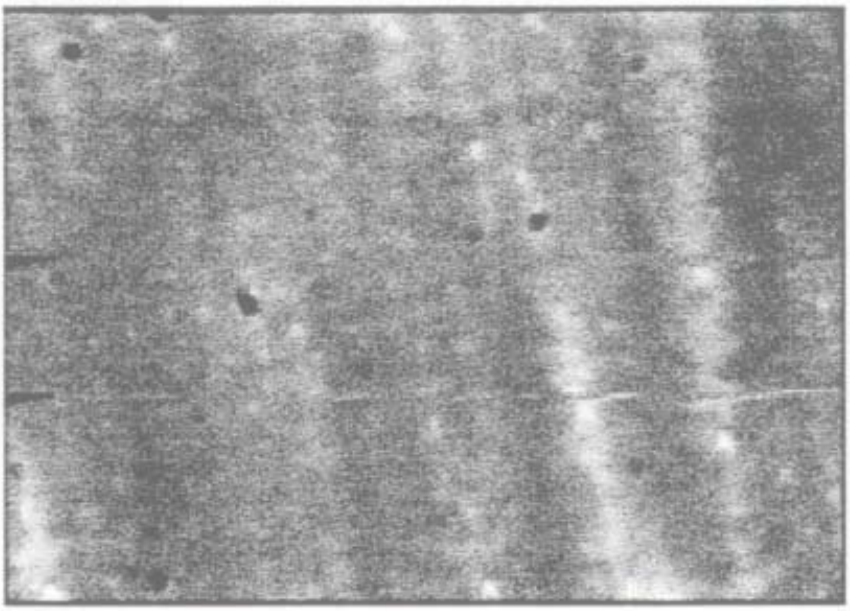

Figure 3a. Microscopic image of part prior to debinding.

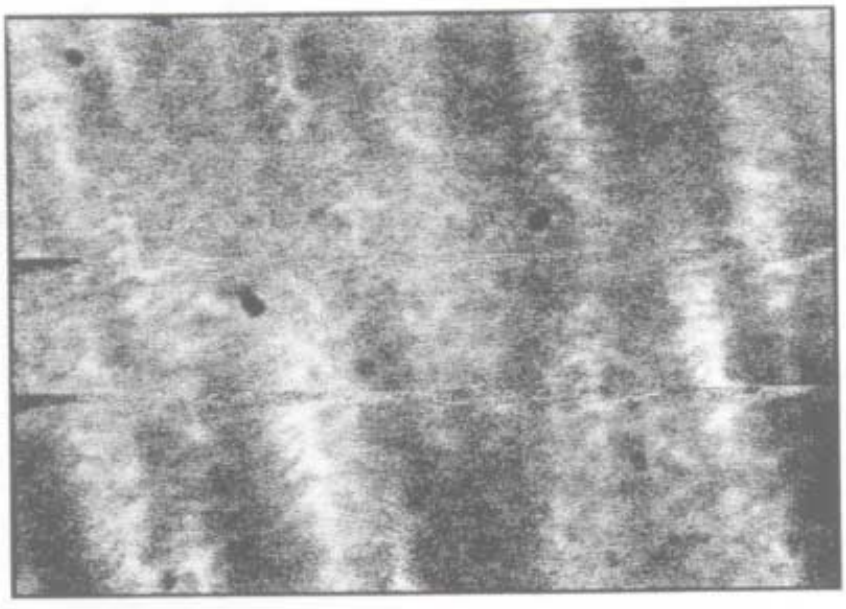

Figure 3b. Same surface after paraffin removal.

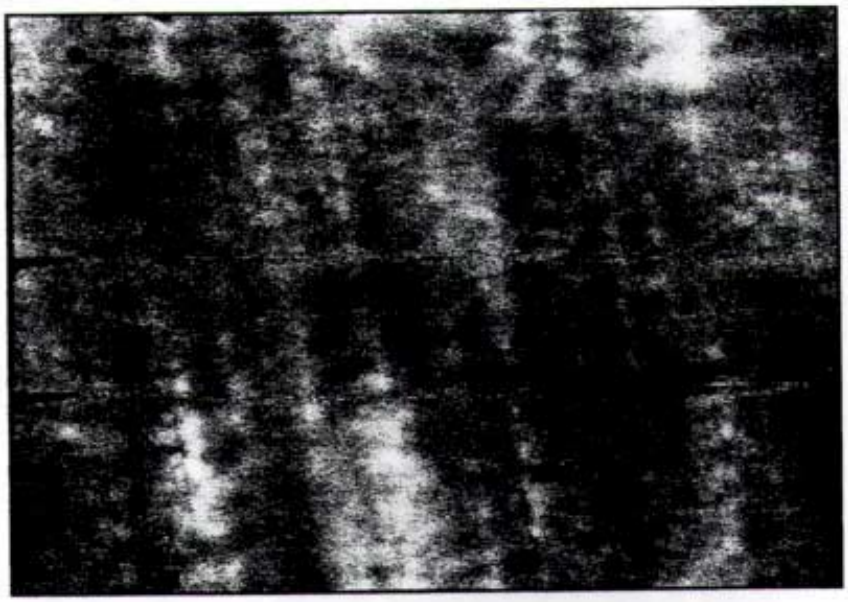

Figure 3c. Surface after polymer removal.

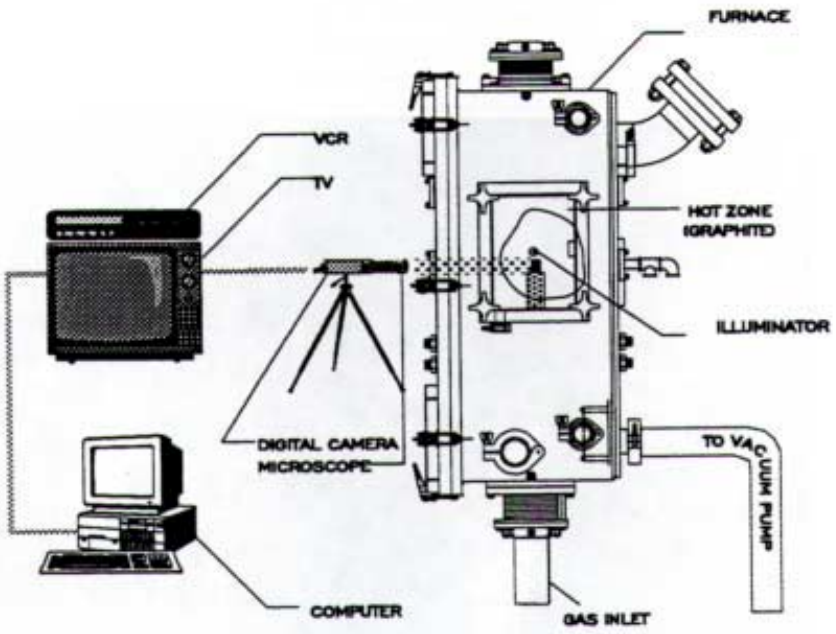

Figure 4. Sintering test setup.

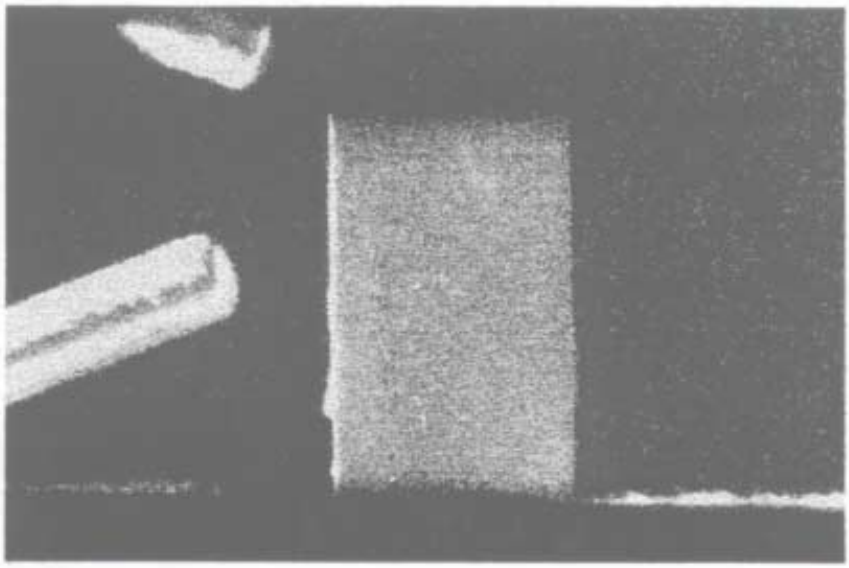

Figure 5. Image of part in furnace prior to start of sinter cycle.

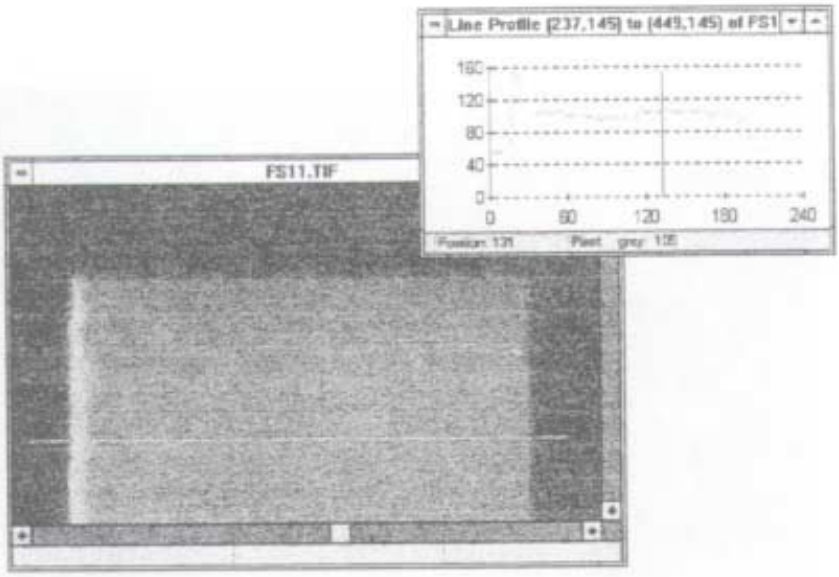

Figure 6. Line profile of part width.

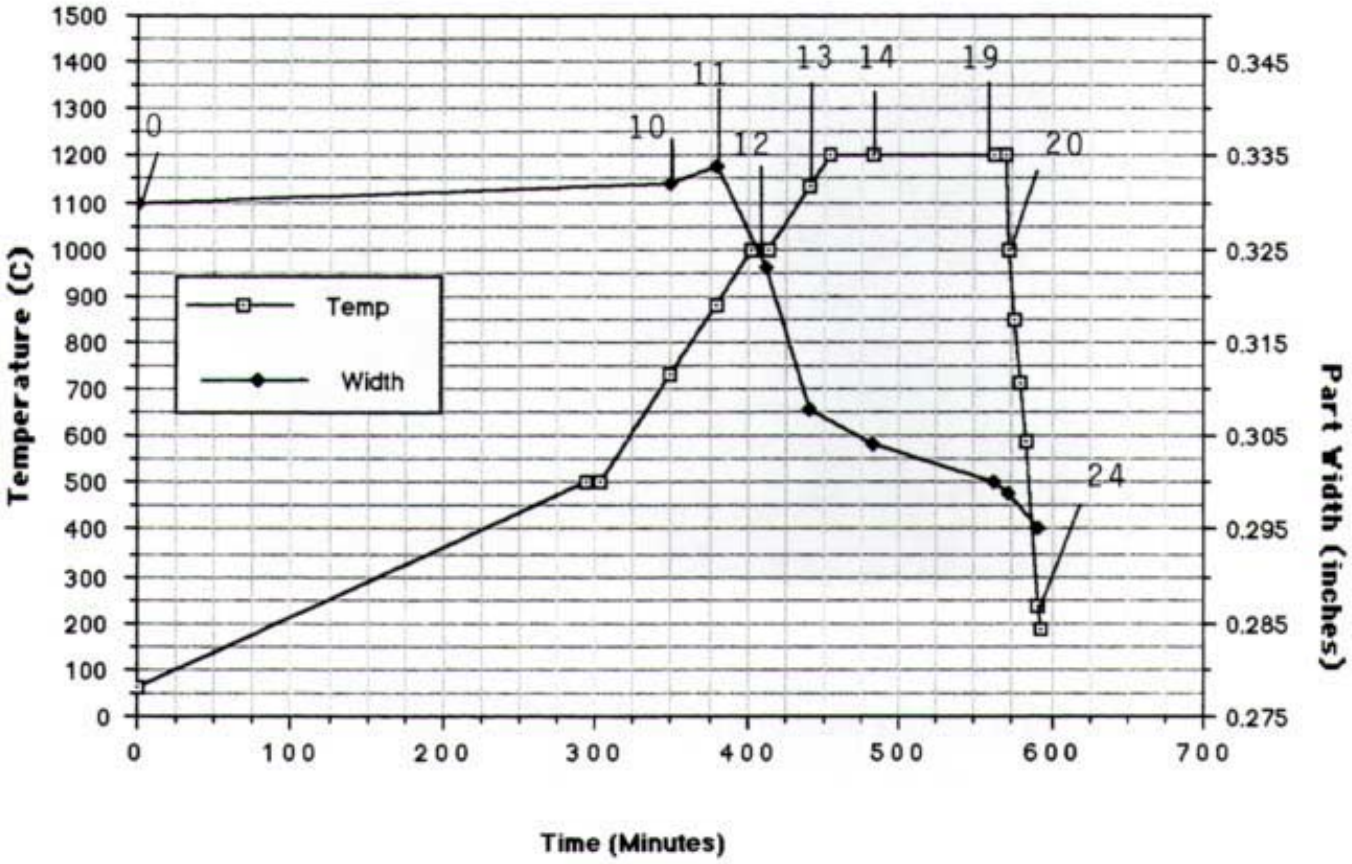

Figure 7. Sinter cycle (gauging) versus part width.

Figure 8. Microscopic image of part surface during presinter ramp.